Science Supporting Online Material.

Grünewald et al., *Three-dimensional Structure of Herpes Simplex Virus from Cryo-electron Tomography.*

Materials and Methods

Strains, cultivation and purification of virions.

African green monkey kidney (Vero) cells (CCL-81; ATCC, Mannasas, VA) and human foreskin fibroblasts (HFT) (*S1*) cells were grown in alpha- minimum essential medium supplemented with 10% fetal calf serum (Invitrogen, Carlsbad, CA) and passaged as described in Desai *et al.* (*S2*). Virus stocks were prepared in Vero cells as described (*S2*). HFT cells were infected with KOS virus at an MOI of 10 PFU/cell. 48 hours after infection, the supernatant culture medium was harvested. The extracellular viruses were concentrated by centrifugation, and loaded on 20-50% sucrose gradients. The virion-containing fraction was recovered, concentrated and resuspended in PBS, and equilibrated overnight.

Controls against compression artifacts.

To address the possibility that the observed asymmetry of the virions (departures from sphericity, eccentric positioning of the nucleocapsid) might be caused by pelleting during sample preparation, we also prepared virions by filtering the medium supernatant through 0.1 μm Durapore filter membranes (Millipore, Bedford, MA). After washes with PBS, the retentate was recovered from the filter membranes and examined by cryo-EM without tilting (Fig. S1A). The eccentricity of the nucleocapsid position relative to the envelope membrane and the asphericity of these particles are apparent in plots of these parameters for a random selection of 41 virions (Figs. S1B, C). An alternative source of asphericity might be compression of virions in response to surface tension effects in the thin film of buffer just prior to freezing. However, since the shortest dimensions of virions

reconstructed in tomograms was not always perpendicular to the ice film, this explanation appears to be ruled out.

Cryo electron microscopy.

A drop of 4 μl virus suspension, prepared by the filtration method, was applied to a freshly prepared holey carbon film. Excess liquid was blotted to a thin film that was vitrified by plunging in liquid ethane. Grids were transferred into a model 626 cryoholder (Gatan, Warrendale, PA) and examined under low dose conditions in a FEI CM120 microscope (FEI, Eindhoven, Netherlands). Micrographs were taken at 22,000x magnification on film and digitized on a SCAI scanner (Z/I Imaging, Huntsville, AL) at a pixel size of 7 µm.

Tomographic data collection.

Typically, a 2.5 µl drop of virus suspension was applied to a freshly prepared holey carbon film, 1 µl of 10-nm colloidal gold particles was added and briefly mixed. Excess liquid was blotted to a thin film that was vitrified by plunging in liquid ethane (ice thickness ~250 nm). Grids were either inserted into a model 626 cryoholder (Gatan, Warrendale, PA) and transferred into a microscope or stored in liquid nitrogen until use. Tilt series were collected automatically (*S3, S4*) at 1.5° increments over an angular range of -63^{o} to $+60^{o}$ on FEI CM120 and CM120-Biofilter microscopes (FEI, Eindhoven, Netherlands). The accelerating voltage was 120 kV and total electron doses were 35-40 electrons/$Å^2$ per series.

Image processing.

Projection alignment, reconstruction, and image processing was done with several software packages, namely Bsoft (*S5*), EM (*S6*), and IMOD (*S7*). Bsoft (*S5*) was used for presegmenting. Visualization and final segmentation was performed in Amira 3.0 (TGS, San Diego, CA). Isosurface rendering for the individual segments was typically done at 0.5 - 0.8 sigma. The averaged capsid (Fig. 4) was thresholded at 1.5 sigma. Before segmentation, the tomograms were subjected to "denoising" by nonlinear anisotropic diffusion (*S8*), using the algorithm in edge enhancement mode for 35 cycles, with the parameter lambda set to 0.5 standard deviations (of the map's voxels).

For capsid averaging and to determine resolution, reconstructed virions were first brought into a common frame of reference corresponding to a view along a 2-fold symmetry axis of the capsid. Capsids from denoised tomograms were roughly segmented by hand and then rotated and shifted to maximize their 3D cross-correlation with an appropriately scaled reference map (*S9*), using the *bfind* routine in Bsoft (*S5*). From this position, the map was rotated 58.3^{o} about the x-axis to align the 5-fold axis with the y-axis. Of the 60 possible symmetry-related views, the one selected was the one that placed the distal pole of the tegument closest to the vertical position (positive y-axis). The same rotations and shifts were also applied to the non-denoised tomograms. 14 virions aligned in this way were averaged. Fivefold symmetrization around the y-axis was applied to increase the signal-to-noise ratio of the tegument-distal pentons and the tegument-proximal pentons, separately (cf. Figs. 4B, 4C).

The capsids were used to assess tomogram resolution by comparing them with the reference density map (*S9*) in terms of the Fourier shell correlation coefficient (threshold 0.3 (*S10*)). For individual virions, these figures should apply to the whole reconstruction. The calculations were performed using the spherical shells between radii of 52 nm and 64 nm, and were performed for each capsid individually for i) unsymmetrized raw; ii) unsymmetrized denoised; iii) icosahedrally symmetrized, raw; and iv) icosahedrally symmetrized, denoised data. The resolution of the averaged capsid, 5.6 nm (Fig. S2), is not compromised by anisotropy because the contributing tomograms sample complementary angular ranges. This value is close to the limits imposed by two optical factors. One is the number of projections (N) in the tilt series, which for a 200 nm diameter (D) particle and a 1.5^{o} angular increment gives a limit of 5.3 nm (=πD/N (*S*3)). The other is the high defocus value used (8μm) which places the point of zero contrast transfer at a resolution of ~ 5.2 nm.

*

Supporting Figures.

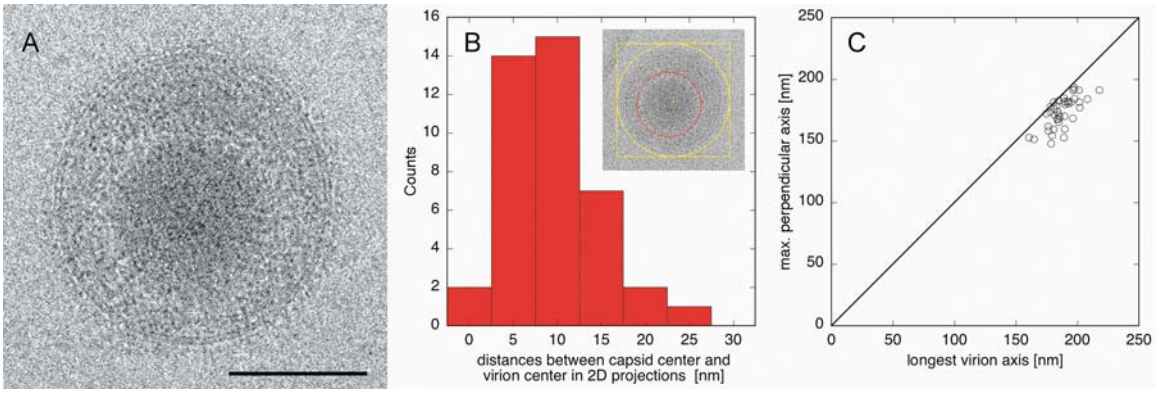

Fig. S1. Asymmetry of HSV-1 virions prepared by filtration, i.e. without exposure to high centrifugal forces. (A) Cryo-electron micrograph of a typical virion embedded in vitreous ice showing an eccentrically positioned capsid in a virion whose overall shape is slightly oval. (B) Histogram for distances between the center of capsid and the center of the virion (n=41). The inset shows a virion with circles around the capsid (red) and around the membrane (yellow) as used for picking the relative centers. Assuming random orientation of the virions in 3D we calculated the average distance between the capsid and virion centers in 3D (based on a mean of curve calculation) as 15 nm. (C) Systematic deviations from sphericity are illustrated in this plot of the longest dimension against the dimension perpendicular to it for same set of filtration-purified virions, as measured from untilted cryo-electron micrographs.

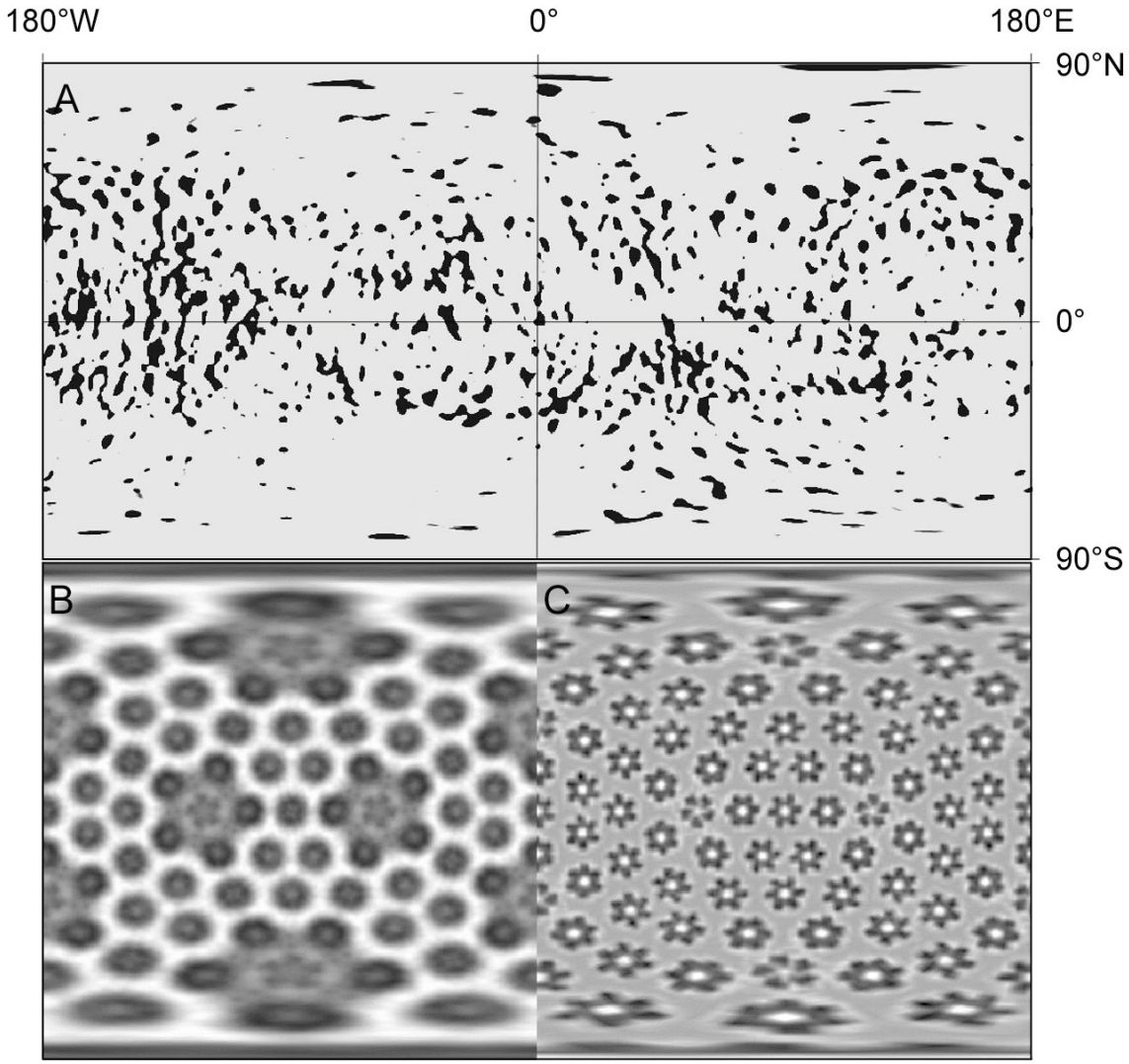

Fig. S2. Mercator projections of spherical shells from HSV-1 particles. (A) Shell of 2.2 nm thickness (i.e. averaged over three radial samples) at a mean radius of 102.5 nm, from a single denoised tomogram of an HSV-1 virion. This shell lies just outside the bilayer membrane The dark features represent glycoprotein spikes. (B) A single shell through the capsid at a radius of 61 nm: left half – from the averaged, icosahedrally symmetrized, tomogram; right half - from the reference cryo-EM density map.

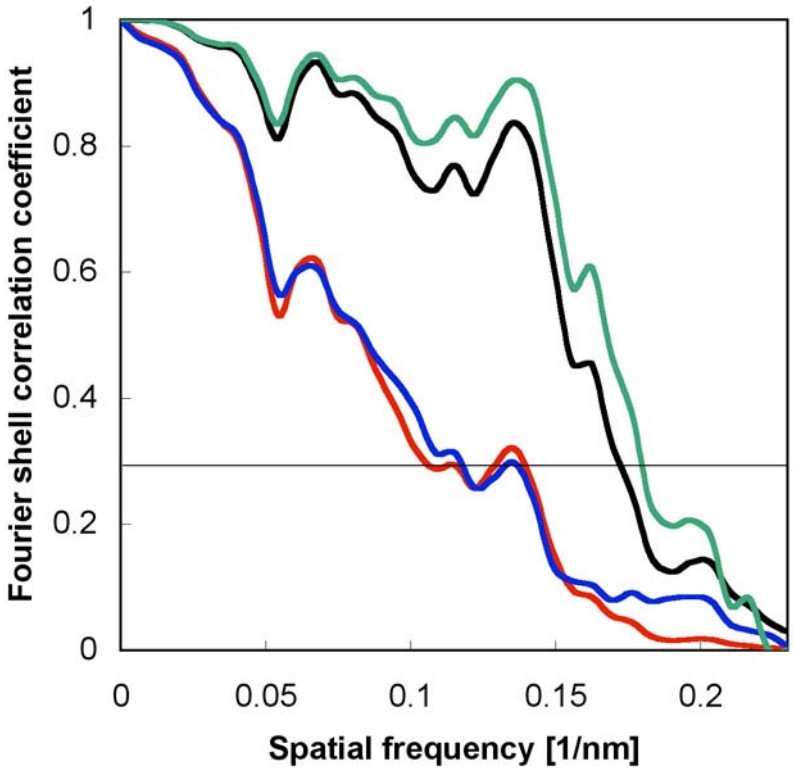

Fig. S3. Resolution curves for tomograms obtained by calculating the Fourier shell correlation coefficient between the capsid portion of the tomogram with the corresponding portion of the reference cryo-EM density map. Resolution is defined as the last point (highest frequency) at which the curve crosses the threshold value of 0.3. The 14 reconstructions were analyzed individually and the average curve for the 10 best reconstructions was calculated (Red) (the next 4 were slightly lower around 0.14 nm^{-1}, although they appeared very similar to the better reconstructions). The same reconstructions were analyzed after denoising (Blue) or icosahedral symmetrization (Black). The 14 reconstructions were aligned, averaged and symmetrized, and the curve for the composite calculated (Green).

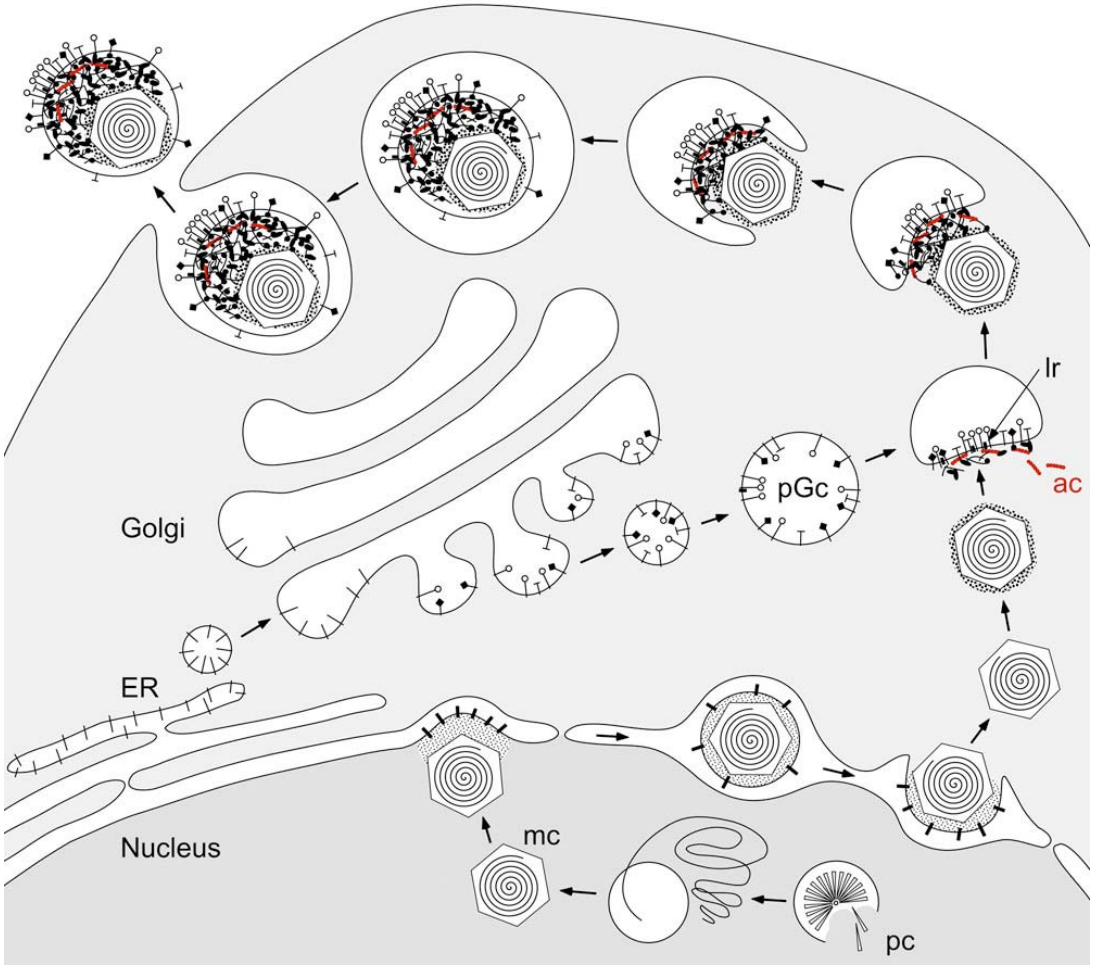

Fig. S4. Egress pathway of HSV-1 nucleocapsids, based on the proposal by Mettenleiter (*S11*). Precursor procapsids (pc) assemble in the nucleus, are then packaged with DNA to produced mature nucleocapsids (mc) that exit the nucleus by envelopment at the inner nuclear membrane to be released into the cytoplasm by de-envelopment at the outer nuclear membrane. Viral glycoproteins accumulate in a post-Golgi compartment (pGc). Secondary envelopment is triggered by interaction of the nucleocapsid and/or attached tegument proteins with glycoprotein endodomains at a specialized site, perhaps involving lipid rafts (lr). Tegument proteins are recruited on to an extending scaffold between the capsid and the membrane in a process that may involve actin microfilaments (ac). The tegumented nucleocapsid is finally internalized into the pGc by pinching off at its proximal pole. Finally, virions are released into extracellular space by fusion of their outer, pGc-derived membrane with the plasma membrane.

References for supporting online material.

S1. W. C. Hahn *et al*., *Nature* **400**: 464, (1999)

S2. P. Desai, N. A. DeLuca, S. Person, *Virology* **247**, 115 (1998).

S3. K. Dierksen, D. Typke, R. Hegerl, W. Baumeister, *Ultramicroscopy* **49**, 109 (1993).

S4. R. Grimm *et al*., *Biophys. J.* **74**, 1031 (1998).

S5. J. B. Heymann, *J. Struct. Biol.* **133**, 156 (2001).

S6. R. Hegerl, *J. Struct. Biol.* **116**, 30 (1996).

S7. J. R. Kremer, D. N. Mastronarde, J. R. McIntosh, *J. Struct. Biol.* **116**, 71 (1996).

S8. A. S. Frangakis, R. Hegerl, *J. Struct. Biol.* **135**, 239 (2001).

S9. N. Cheng *et al*., *J. Virol.* **76**, 7855 (2002).

S10. A. Miyazawa, Y. Fujiyoshi, M. Stowell, N. Unwin, *J. Mol. Biol.* **288**, 765 (1999).

S11. T. C. Mettenleiter, *J. Virol.* **76**, 1537 (2002).